Kinetic particle simulation of discharge and wall erosion of a Hall thruster

Shinatora Cho, Kimiya Komurasaki, and Yoshihiro Arakawa

Citation: Phys. Plasmas **20**, 063501 (2013); doi: 10.1063/1.4810798
View online: http://dx.doi.org/10.1063/1.4810798
View Table of Contents: http://pop.aip.org/resource/1/PHPAEN/v20/i6
Published by the American Institute of Physics.

Kinetic particle simulation of discharge and wall erosion of a Hall thruster

Shinatora Cho,[1,a)] Kimiya Komurasaki,[2] and Yoshihiro Arakawa[2]
[1]Japan Aerospace Exploration Agency, 7-44-1 Jindaiji, 182-8522 Chofu, Tokyo, Japan
[2]The University of Tokyo, 7-3-1 Hongo, 113-8656 Tokyo, Japan

(Received 18 March 2013; accepted 7 May 2013; published online 12 June 2013)

The primary lifetime limiting factor of Hall thrusters is the wall erosion caused by the ion induced sputtering, which is predominated by dielectric wall sheath and pre-sheath. However, so far only fluid or hybrid simulation models were applied to wall erosion and lifetime studies in which this non-quasi-neutral and non-equilibrium area cannot be treated directly. Thus, in this study, a 2D fully kinetic particle-in-cell model was presented for Hall thruster discharge and lifetime simulation. Because the fully kinetic lifetime simulation was yet to be achieved so far due to the high computational cost, the semi-implicit field solver and the technique of mass ratio manipulation was employed to accelerate the computation. However, other artificial manipulations like permittivity or geometry scaling were not used in order to avoid unrecoverable change of physics. Additionally, a new physics recovering model for the mass ratio was presented for better preservation of electron mobility at the weakly magnetically confined plasma region. The validity of the presented model was examined by various parametric studies, and the thrust performance and wall erosion rate of a laboratory model magnetic layer type Hall thruster was modeled for different operation conditions. The simulation results successfully reproduced the measurement results with typically less than 10% discrepancy without tuning any numerical parameters. It is also shown that the computational cost was reduced to the level that the Hall thruster fully kinetic lifetime simulation is feasible. © *2013 AIP Publishing LLC*. [http://dx.doi.org/10.1063/1.4810798]

I. INTRODUCTION

A Hall thruster[1] is one of the most successful electric propulsion for satellite station keeping and orbit transfer missions for its high specific impulse. The discharge plasma of Hall thrusters has the interesting characteristic that only the electrons are magnetically confined and forming electrostatic field for ion acceleration, whereas the ions are not confined by the magnetic field. Moreover, the range of plasma parameters tend to be wide that the plasma is weakly ionized with weak magnetic confinement (electron Hall parameter $\Omega_e < 100$) at the upstream channel, whereas it is close to fully ionized plasma with strong magnetic confinement at the downstream channel. These characteristics make the physics of Hall thruster discharge complex and uneasy to model.

As is the case for other electric propulsion systems, though Hall thrusters can achieve high specific impulse, the thrust they can perform is smaller than that of the chemical propulsion systems by several orders of magnitude. Therefore, Hall thrusters are required to operate for more than thousands hours to complete missions that the lifetime performance is essentially important for their mission applications. The primary lifetime limiting factor of Hall thruster propulsion systems is the discharge channel wall erosion (usually boron nitride, BN) caused by ion sputtering. Wall erosion leads to the recession of thruster channel wall surface, and finally, the magnetic circuit will directly be exposed to the plasma, which is defined to be the end-of-life (EOL) state of the thruster. Thus, lots of long-duration tests[2–4] have been conducted in order to evaluate and improve the lifetime performance of Hall thrusters. In practice, the necessary testing time and cost is the major obstacle for the lifetime extension or thruster optimization. The long-time endurance test of Hall thrusters typical requires accumulative operation over thousands of hours and immense testing cost which makes the repetitive experiment with different configurations practically impossible. Particularly, the development of high power Hall thruster is attracting increasing interest for which the necessary testing cost significantly increases.[5] Therefore, the development of numerical lifetime simulation model is necessary for lifetime performance improvement and further mission applications of Hall thrusters.

A number of numerical studies have been devoted for Hall thruster modeling. The most successful and most used numerical model is Hybrid particle-in-cell (PIC), which treats the electrons as fluid and heavy particles directly as particle.[6] Particularly, the quasi-one-dimensional hybrid PIC model called HPHall developed by Fife[7] was employed and improved by different institutes because of its robustness, accuracy, and low computational cost.[8–10] These models were also implemented for wall erosion and lifetime simulations.[11–13] However, it is necessary for these fluid-based models to use quasi-neutrality and Maxwellian electron energy distribution function (EEDF) assumptions throughout the calculation domain. These assumptions make it impossible to conduct self-consistent dielectric wall sheath modeling, despite of their significant impact on the wall erosion. Namely, the main wall erosion process of Hall thrusters is known to be sheath-induced phenomena that the ion-attracting pre-sheath and ion acceleration inside the sheath play dominant roles in prescribing the wall-impinging ion flux and energy, respectively.

a)Electric mail: choh.shinatora@jaxa.jp

On the other hand, kinetic models which can capture the non-quasi-neutral and non-equilibrium physics were also developed so far. The fully Kinetic PIC Direct Simulation Monte Carlo (DSMC) model[14] tracing the trajectory of all kinds of particles was first applied to Hall thrusters by Hirakawa[15] and was further developed and improved.[16–21] It is well known that the space and time resolution are, respectively, restricted by the Debye length and the plasma frequency in fully kinetic PIC DSMC models, which makes the simulation extremely computationally expensive. In fact, the previous fully kinetic studies using only true physical properties spent months for the simulation over the characteristic time of the Hall thruster discharge ($\sim 100\,\mu$s).[20,21] Consequently, this major drawback of PIC-DSMC model makes it difficult to conduct parametric study or the wall geometry time-evolution modeling, and there was no successful Hall thruster lifetime simulation conducted so far to be best of our knowledge. Naturally, notable techniques for speeding up the computation were developed and investigated. The artificial mass ratio and permittivity manipulations are the most used acceleration technique,[15,16,18,19] whereas Taccogna presented an acceleration method model by scaling down the thruster size according to a self-similarity law.[17] As the side effect of these techniques, however, they can cause unrecoverable change of physics especially if multiple manipulations were employed at the same time.

The purpose of this study is to develop a *r-z* two-dimensional fully kinetic PIC DSMC model for the numerical reproduction and prediction of Hall thruster lifetime with improved accuracy than Hybrid PIC models. Although another option of fully kinetic model can be the direct simulation of Vlasov equation,[22] it was not adopted because of its even higher computational cost then PIC model. Unfortunately, it is considered to be unfeasible to accomplish the full-PIC lifetime simulation within an acceptable computational cost without implementing any acceleration technique. Therefore, we adopted the artificial mass ratio manipulation, though no other artificial techniques were employed with the intention of better preservation of physics. Furthermore, it was considered that the mass ratio models used in previous studies were inappropriate for wall erosion modeling because either the wall-impinging ion flux[16] or the electron mobility[18] was unpreserved. Therefore, a new physics recovering model for the mass ratio was presented considering the characteristics of Hall thruster discharge plasma. The detailed simulation model and its validation rather than the lifetime simulation result[23] is mainly elaborated in this paper. Section II describes the simulation model, and Sec. III provides the validation of the model. In Sec. IV, the simulation results was presented and was discussed.

II. SIMULATION MODEL

A. Overview of simulation model

A fully kinetic PIC model including two dimensions in space (*r-z*) and three dimensions in velocity (*r-z-θ*) is presented. The very basic governing equations start from the Boltzmann equation and the Maxwell equation. Assuming the time-invariant magnetic field, the system reduces to the Poisson equation and the equation of motion for each particle

$$\Delta\phi = \rho/\varepsilon, \tag{1}$$

$$m\dot{\boldsymbol{v}} = q(\boldsymbol{E} + \boldsymbol{v} \times \boldsymbol{B}), \tag{2}$$

where, ϕ is potential, ρ is space charge, ε is permittivity, $\boldsymbol{v}$ is velocity, m is mass, q is charge of the species, $\boldsymbol{E}$ is electric field, and $\boldsymbol{B}$ is magnetic flux density. The trajectories of all the particle species are directly traced according to the field, whereas the field is calculated according to the space charge weighted from the particles.

The numerical conditions used in this study are summarized in Table I. Uniform rectangular grid with spacing of 2.0×10^{-4} m in a cylindrical coordinate was adopted. The computational time-step was 1.0×10^{-11} s for both the field and the particle dynamics computation. Note that this time step is the value without the acceleration of the computation via artificial mass ratio. As for the computation speeding up technique, first the artificial mass ratio manipulation was adopted that the mass of electron was magnified by the factor of 2500. In addition, the concept of macro particle[16] was used that in nominal condition, one simulation particle represents 2.0×10^7 real particles ($\sim$200 particles per cell in average for each species) in order to avoid calculating unnecessarily too many particles. Nevertheless, the technique of artificial permittivity and self-similarity scaling was not used in order to avoid summing up nonlinear artificial correction effects. Because the simulation model ignores azimuthal fluctuations, the Bohm diffusion was employed to compensate for the reduced electron mobility across the magnetic field. Although the anomalous electron transport remains to be an open question that there are various discussions about which and how to explain and employ the model,[24–26] it is beyond the scope of this work to further investigate on the Bohm diffusion model itself. Thus, the conventional Bohm diffusion model with the constant coefficient of 1/16 was employed. The convergence of

TABLE I. Simulation conditions.

Item	Value	Parametric study presented
Timestep	1.0×10^{-11} s	
Grid spacing	2.0×10^{-4} m	X
Artificial mass ratio	Electron mass multiplied by $f^2 = 2500$	X
Artificial permittivity	NOT used	
Self-similarity scaling	NOT used	
Macro particle	2.0×10^7 real particles	X
Bohm diffusion coefficient	1/16	
Particle species	e^-, Xe, Xe^+, Xe^{++}	
Collision	e^-–Xe elastic scattering e^-–Xe excitation e^-–Xe ionization e^-–Xe^+ ionization	

computation was judged by whether the total particle number and other macro discharge parameters reached steady states (or quasi-steady operation with discharge oscillation) or not. Typically, computation over 0.1 ms was enough to reach a converged state. The entire code was parallelized by using message passing interface (MPI) and free library PETSc, and the simulation was conducted by a 12 core 3.4 GHz CPU workstation. In order for the validation of the model, parametric studies were conducted for the mass ratio, grid spacing, and the size of super particle and will be presented in chapter III.

B. Mass ratio model

The technique of artificial mass ratio manipulation was implemented to speed up the simulation for most of the previous Hall thruster fully kinetic simulations.[15,16,18,19] The concept is that the real mass ratio was reduced by the artificial mass factor f^2 as Eq. (3)

$$\left(\frac{m_i}{m_e}\right)_{real} = f^2 \left(\frac{m_i}{m_e}\right)_{artificial}. \tag{3}$$

Because the plasma of Hall thrusters is magnetically confined only for electrons but not for ions, there are two different ways of implementation. One is to reduce the mass of heavy particles by the factor of $1/f^2$ to accelerate the convergence of simulation,[16,19] and the other is to magnify the electron mass by the factor of f^2 to reduce the plasma frequency and afford larger time-step.[18] Both methods need physics recovering model and have their own merits and demerits. According to Szabo,[16] the corrections for the ion acceleration method are

$$\dot{m}_n \rightarrow \dot{m}'_n = f\dot{m}_n, \tag{4}$$

$$B_i \rightarrow B'_i = (1/f)B_i, \tag{5}$$

$$\sigma_{en} \rightarrow \sigma'_{en} = (1/f)\sigma_{en}, \tag{6}$$

where, $\dot{m}_n$ is propellant mass flow rate, B_i is magnetic flux density for ions, σ_{en} is cross section for electron neutral collision, and dash denotes the parameter was corrected. Equations (4) to (6), respectively, denote the corrections for the preservation of propellant molar flow rate, ion Larmor radius, and collision cross-section. In this way, the necessary number of iterations to reach convergence is reduced by the factor of $1/f$. The demerit of this method is that the ion wall loss flux is theoretically not preserved so that additional artificial manipulation is necessary to model the ion-wall interaction. Indeed, the wall loss ions were selectively reflected back to the plasma in previous studies, which reduces the accuracy and self-consistency of the simulation. Thus, this ion-acceleration method was not adopted in this study.

On the other hand, according to Yokota,[18] the corrections for the electron-deceleration method are

$$B_e \rightarrow B'_e = fB_e, \tag{7}$$

$$\sigma_{en} \rightarrow \sigma'_{en} = f\sigma_{en}, \tag{8}$$

where, B_e is magnetic flux density for electron. Equations (7) and (8), respectively, denote the corrections for the preservation of electron Larmor radius and collision cross-section. In this way, the electron speed and hence the computational cost will be reduced by the factor of $1/f$ because the acceptable time step will be enlarged by the factor of f. The merit of this method is that as long as the mobility or diffusion coefficient of electron is preserved, the numerical change of plasma properties is considered to be insignificant. Thus, the wall erosion rate is considered to be preserved better and more appropriate for lifetime simulation than ion acceleration method. Nevertheless, one of the major limitations of this method is that the electron Hall parameter Ω_e is unpreserved

$$\Omega_e = \frac{eB_e}{m_e\nu_{en}} \rightarrow \Omega'_e = \frac{eB'_e}{m'_e\nu_{en}} = \frac{1}{f}\Omega_e, \tag{9}$$

where, ν_{en} is electron-neutral scattering collision frequency. Generally saying, electron Hall parameter indicates the strength of electron confinement by magnetic field and does not affect the classical electron mobility μ_e in this model as long as $\Omega'^2_e \gg 1$ is satisfied

$$\mu_e = \frac{\frac{e}{m_e\nu_{en}}}{1+\Omega_e^2} \rightarrow \mu'_e = \frac{\frac{e}{m'_e\nu_{en}}}{1+\Omega'^2_e} \approx \mu_e. \tag{10}$$

However, this condition is sometimes not satisfied at the Hall thruster near-anode region where the magnetic field is weak and the neutral density is high. Fig. 1 illustrates the impact of artificial factor on the electron Hall parameter and mobility at near-anode region ($B = 6$ mT, $\nu_{en} = 3 \times 10^7$ Hz). When artificial factor becomes greater than about 1000, Hall parameter comes close to unity and electron mobility begins to drastically decrease from its real value with the increase of artificial factor. This means the physics of electron transport across the magnetic field will be distorted by the mass ratio manipulation.

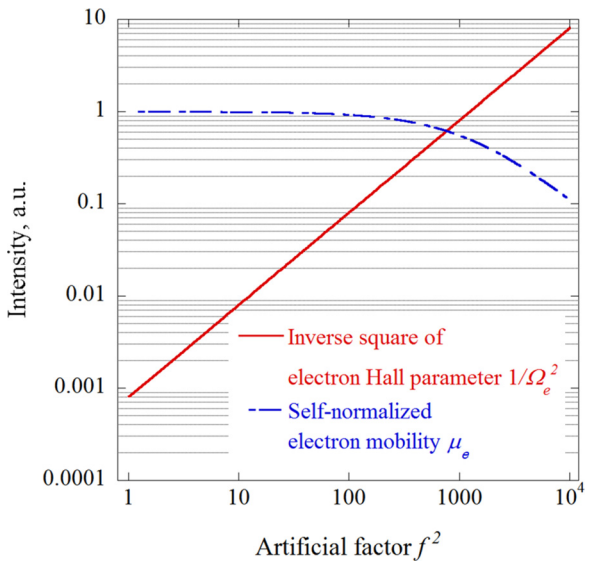

FIG. 1. Electron Hall parameter and mobility.

The figure also shows that for the typical operation condition stated above, it is favorable to use artificial factor not greater than 100 to avoid the unrecoverable change of physics, which is much smaller than the factor used in previous studies. Naturally, however, reducing the artificial factor from 2500 to 100 immediately increases the computation cost by almost an order of magnitude, which is unfavorable for costly lifetime simulation or for the simulation of high power Hall thrusters. Therefore, a new modified mass ratio correction models were presented in this study.

The presenting idea is to reduce the change of electron Hall parameter for better preservation of mobility at the expense of unpreserved Larmor radius r_L

$$B_e \rightarrow B'_e = f_B B_e, \tag{11}$$

$$\nu_{en} \rightarrow \nu'_{en} = (f_B/f)^2 \nu_{en}, \tag{12}$$

where f_B ($<f$) is correction factor for magnetic field. With this new correction model, the electron Hall parameter is reduced by the factor $1/f_B$, and Larmor radius is increased by the factor of f/f_B from their real value that both of these parameters are not preserved. However, the effect of these changes can be minimized by choosing the most appropriate mass ratio f_B/f. Fig. 2 presents the impact of factor f_B on the Hall parameter and Larmor radius for typical operation conditions with the artificial factor of $f=2500$. Here, $L=7$ mm is the discharge channel length, B_{min} is the minimum magnetic flux density inside the channel (usually at the vicinity of anode), and B_{acc} is the magnetic flux density at the ion acceleration region. Both of the parameter $1/\Omega'^2_e$ and r_L/L should be small enough than unity in order to avoid significant change of electron transportation physics. Thus, the best fraction of f_B/f can be determined by the point minimizing both parameters. Practically, the fraction can be decided by the area enclosed by the four lines on Fig. 2, for example, considering a certain range of thruster operation conditions.

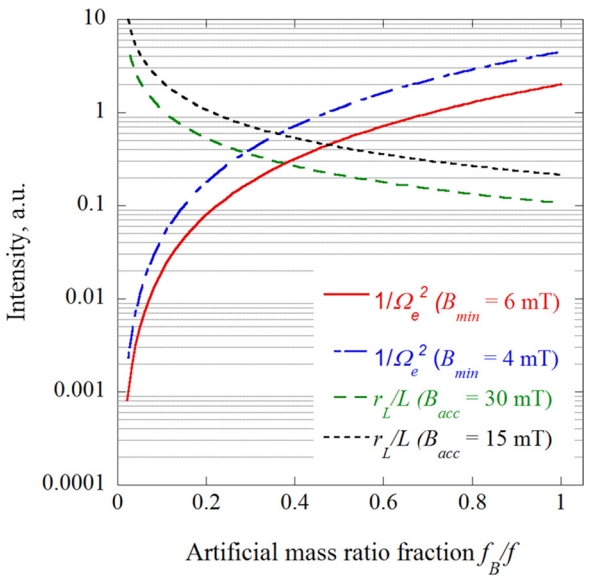

FIG. 2. Mass ratio fraction dependence of effective electron Hall parameter and Larmor radius (scattering collision frequency of 3×10^7 Hz and electron temperature of 30 eV was assumed).

Note that the mass ratio correction model recovers to the model used in previous study, if $f_B/f = 1$ is employed. It is emphasized that the mass ratio fraction is not intended to be used as an adjustable "tuning parameter." The impact of mass ratio fraction on the simulation result was investigated and presented in Sec. III B.

Table II summarizes the numerical manipulations and the change of plasma parameters. The major advantage of the presented electron deceleration model is that the physics of electron transport across the magnetic field is preserved even for the weakly magnetically confined plasma (e.g., $\Omega_e < 100$). This is critically important for Hall thruster modeling because the magnetic confinement in the channel upstream region is inevitably weak, and the plasma properties of the upstream channel essentially have predominant influence on that of the downstream and hence the entire thruster. Although the Larmor radius will be enlarged in the model, this side effect is insignificant because the relationship of $\lambda_D \ll r'_L \ll L$ is satisfied. Furthermore, the necessary physics recovering corrections are determined by the thruster geometry and operation conditions so that the self-consistency of the simulation is not reduced. Nevertheless, the limitations of the presented model are first, the physics of electron-scale instability will be numerical changed because of the unpreserved electron cyclotron frequency and plasma frequency. Second, the effectiveness of the model is reduced for very weakly magnetically confined plasma (e.g., $\Omega_e < 10$) because the acceptable artificial mass factor will be smaller. Finally, it is notable that because of the reduced scattering collision frequency, employing small mass fraction (e.g., $f_B/f < 0.1$) can cause insufficient relaxation of electron energy and result in the unpreserved EEDF or the numerical instability, though this is not the case for nominal Hall thruster operation.

C. Field solver

It is well-known that for the explicit formulation of Vlasov-Maxwellian equations, the time-step Δt and grid spacing Δx are restricted by the electron plasma frequency ω_{pe} and Debye length λ_D, respectively.[14] In order to overcome these computationally expensive restrictions, semi-implicit field solver was adopted[27]

TABLE II. Summary of numerical manipulations and plasma parameters (dash denotes the modified quantities).

	Quantities	Modifications
Numerical manipulations	Time step	$\Delta' t = f\Delta t$
	Electron mass	$m' = f^2 m$
	Magnetic flux density for electron	$B'_e = f_B B_e$
	Collision cross-section	$\sigma'_{en} = f\sigma_{en}$
	Scattering collision frequency	$\nu'_{en} = (f_B/f)^2 \nu_{en}$
Plasma parameters	Debye length	$\lambda'_D = \lambda_D$
	Electron Hall parameter	$\Omega'_e = (1/f_B)\Omega_e$
	Larmor radius	$r'_L = (f/f_B) r_L$
	Electron mobility	$\mu'_e = \frac{1+\Omega_e^2}{f_B^2+\Omega_e^2}\mu_e \approx \mu_e$
	Electron cyclotron frequency	$\omega'_c = (f_B/f^2)\omega_c$
	Plasma frequency	$\omega'_{pe} = (1/f)\omega_{pe}$

$$\nabla \cdot (\varepsilon \boldsymbol{E}^{n+1}) = \rho^{n+1} \cong \rho^n - \nabla \cdot \boldsymbol{j}^{n+1} \Delta t, \tag{13}$$

$$\boldsymbol{j}^{n+1} \cong \boldsymbol{j}_i^n + (1 - \nu_{en}^n \Delta t)\boldsymbol{j}_e^n + \frac{e^2 n_e^n \Delta t}{m_e} \boldsymbol{E}^{n+1} + \frac{e\Delta t}{m_e}(\boldsymbol{j}_e^n \times \boldsymbol{B}), \tag{14}$$

where $\boldsymbol{j}$ is the current density, ν_{en} is the electron-neutral scattering collision frequency, n_e is the electron density, and the superscript n is the time index. Assuming Eq. (15), the system reduce to Eq. (16)

$$\nabla \cdot (n_e^n \boldsymbol{E}^{n+1}) \cong n_e^n \nabla \cdot \boldsymbol{E}^{n+1}, \tag{15}$$

$$\nabla \cdot (\varepsilon \boldsymbol{E}^{n+1}) \cong \frac{1}{1 + (\omega_{pe}\Delta t)^2} \left\{ \rho^n - \nabla \cdot \left[\boldsymbol{j}_i^n + (1 - \nu_{en}^n \Delta t)\boldsymbol{j}_e^n + \frac{e\Delta t}{m_e}(\boldsymbol{j}_e^n \times \boldsymbol{B}) \right] \Delta t \right\}. \tag{16}$$

In Eq. (16), obviously the fluctuations of the electric field on the order of plasma frequency will be time-averaged and smoothed away. Note that all of the parameters related to the mass ratio manipulation were corrected, and the vector term of currents $\boldsymbol{j}_i^n$ and $\boldsymbol{j}_e^n$ were derived by integrating the information of every simulation particle.

By using this semi-implicit field solver, the simulation is numerically stable even if the time-step and grid spacing do not satisfy the criteria of plasma frequency and Debye length, which can significantly reduce the computational cost and makes it possible to eliminate the unphysical artificial electric permittivity. Practically, now the time resolution is restricted by the electron cyclotron frequency, whereas the spatial resolution is regulated by the thickness of dielectric wall sheath. Nevertheless, the limitation of this semi-implicit method will be its incapability of resolving the instability whose frequency is on the order of plasma frequency.

This method was first applied to Hall thruster simulation by Adam and produced promising results,[20] though the wall sheath area was not treated his work. Thus, in this study, the model was improved in the way that the dielectric wall and the wall sheath area were included into the calculation domain for the wall erosion modeling. The field inside the insulator wall was also computed accordingly and hence, the electric permittivity ε is not always equal to the vacuum permittivity

$$\varepsilon = [\gamma + (1 - \gamma)\varepsilon_{BN}]\varepsilon_0, \tag{17}$$

$$\gamma = \frac{V_{vaccum}}{V_{vaccum} + V_{BN}}, \tag{18}$$

where, γ $(0 \le \gamma \le 1)$ is volume fraction of the cell and V represents the volume.

Fig. 3 summarizes the boundary conditions for the field solver. Colored square represents the calculation domain. No special boundary conditions were imposed upon the insulator channel wall surface that the wall is only expressed by the difference of electric permittivity and the boundary conditions for particles, though the charge accumulated on the wall was taken into consideration and was treated the same as the space charge at the vacuum. Neumann condition was imposed upon the most part of the channel wall back surface except the magnetic circuit boundary, where Dirichlet condition of 0 V was imposed.

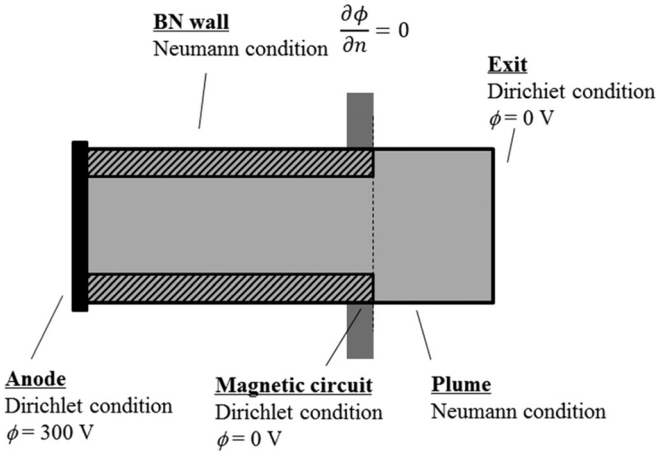

FIG. 3. Boundary conditions for field solver.

D. Particle dynamics

The particle trajectories of all species are calculated according to the equation of motion by 4th order Runge-Kutta method. Fig. 4 summarizes the boundary conditions for all kinds of particles. Neutrals and ions are thermalized on the wall surface with the accommodation coefficients of 0.9 and 0.5, respectively.[16] Charge is accumulated on to the wall surface when charged particles collide with the wall, and the accumulated charge was taken into consideration to the field calculation. Only electron induced secondary electron emission (SEE) was modeled, whose emission yield δ can be written as[28]

$$\delta = (T_e/35)^{0.5}, \tag{19}$$

where T_e is the incident electron temperature in eV. Electrons are injected from the plume and exit boundary to sustain the local quasi-neutrality with initial energy of two eV.

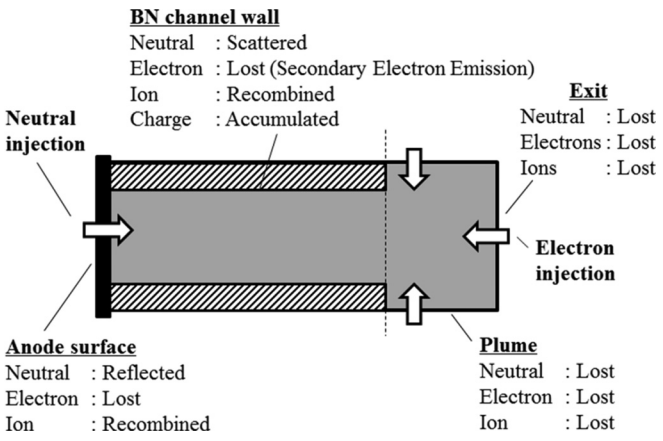

FIG. 4. Boundary conditions for particles.

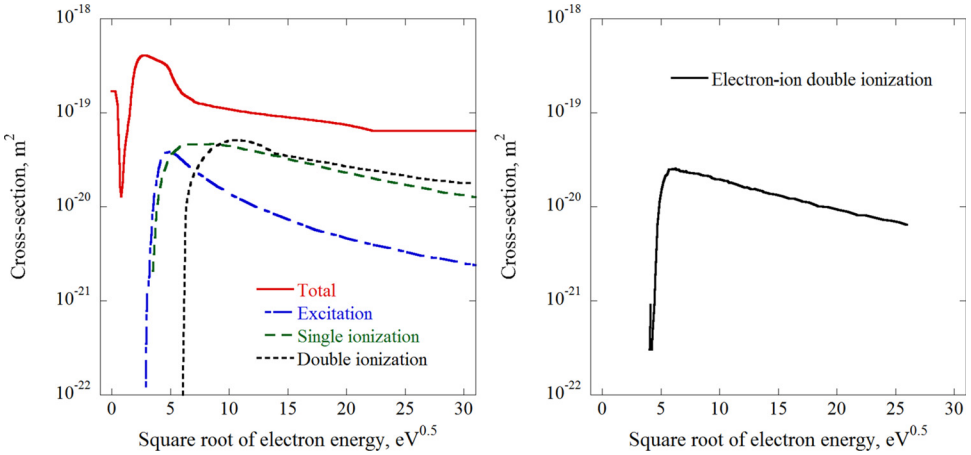

FIG. 5. Collision cross-section model for electron neutral collision (left) and electron ion collision (right).

E. Inter particle collisions

Inter-particle collisions were modeled by Direct Simulation Monte Carlo (DSMC). Only four kinds of dominant particles; ions, doubly charged ions, electrons, and neutrals were simulated, and corresponding Xe–e$^-$ ionization collisions, Xe$^+$–e$^-$ ionization collisions, Xe–e$^-$ excitation, and Xe–e$^-$ elastic scattering were modeled. The fractions of triply or higher charged ions were considered to be small and were neglected. The cross-section models used in this study are the curve fit to the experimental results,[29–33] which were summarized in Fig. 5.

The charge exchange collisions (CEX) between the high energy ions and the low energy neutrals were omitted in the model because their collision cross-section was considered to be negligibly small according to Szabo.[16] However, recent study suggests that these CEX collisions can be potentially important interactions for the thruster performance.[22] Therefore, implementing CEX collision models is considered to be a possible near-future development because it is not difficult to include one within the DSMC framework.

According to the previous study,[18] the virtual collision frequency ν_{Bohm} accounts for the Bohm diffusion can be written as

$$\nu_{Bohm} = \frac{1}{16}\frac{eB}{m_e}, \tag{20}$$

where, 1/16 is the assumed Bohm diffusion coefficient. Note that this virtual collision frequency was calculated by using corrected quantities according to the mass ratio model described in Sec. II B and was implemented by Monte Carlo Collision (MCC).

F. Sputtering model

Channel wall erosion rate was calculated according to the ion inflow to the wall and the sputter yield. It is well known that sputtering yield has both incident energy and angle dependence that the sputtering yield model can be written as

$$Y(E_i, \theta_i) = Y_n(E_i) \times Y_\theta(\theta_i), \tag{21}$$

where $Y_n(E_i)$ is the normal sputtering yield as the function of incident ion energy, and $Y_\theta(\theta_i)$ is the normalized angular dependence of sputtering yield. The employed angular dependence model is presented in Ref. 23, which is the 4th order polynomial fitting to the Garnier's experimental result.[34] The horizontal axis is the angle measured from the perpendicular direction from the target surface that the zero degree means the normal incident. The presented angular sputtering yield was normalized by the normal sputtering yield. There exists threshold energy for sputtering that no sputtering occurs if the energy of incident ion is lower than this threshold. Although there are lots of experimental and numerical studies about this threshold energy, unfortunately the accurate threshold energy for Xe-BN sputtering still remains in vague. According to Yamamura and Tawara model,[35] the ion energy dependence of normal sputtering yield can be written as

$$Y_n(E_i) = \frac{AE_i^{0.5}}{1 + BE_i^{0.3}}\left(1 - \sqrt{\frac{E_{th}}{E_i}}\right)^{2.5}, \tag{22}$$

where E_i is the incident ion energy, E_{th} is the threshold energy of sputtering, A and B and arbitrary parameters. It is beyond the scope of this thesis to investigate about the most appropriate sputtering model so that the employed model was decided by the fitting to the Rubin's experiment result[36] with the assumption that the threshold energy equals to 25 eV. Accordingly, the arbitrary fitting parameters were calculated as $A = 3.64$ and $B = 150.0$. Fig. 6 illustrates the normal sputtering yield model adopted in this study.

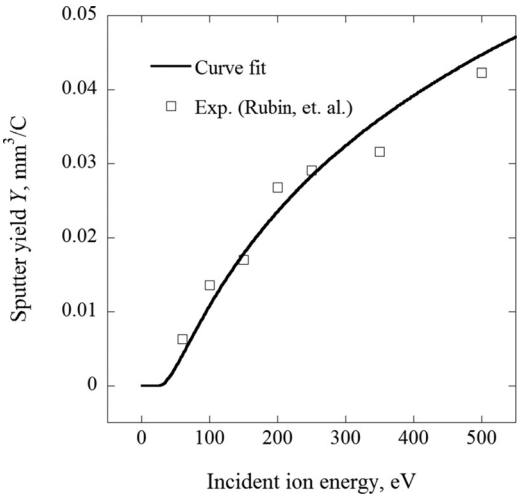

FIG. 6. Angular sputtering yield model.

G. Hall thruster and thrust performance

A laboratory model 600 W-class magnetic layer type Hall thruster[37] (UT-SPT-62) was modeled in this study. The thruster's channel inner and outer diameters are, respectively, 48 mm and 62 mm, and the channel length was 21 mm. The magnetic circuit of the thruster consists of soft iron pole piece and solenoid coil, and the maximum magnetic flux density was about 14 mT at the channel center for the condition of magnetic coil current 1.0 A. The magnetic field is calculated in advance by using free software FEMM (Finite Element Method Magnetics) and imported into the simulation.

Because the computational area does not necessarily covers the 100% of the ion acceleration but only reaches to the 10 mm downstream from the channel exit, the thrust force tend to be underestimated than its true value if it was evaluated by integrating the axial velocity of ions ejected from the exit and plume boundaries. Thus, the thrust force was evaluated in terms of electromagnetic force produced by Hall current, which can be computed as

$$T = \int J_H \times \boldsymbol{B}\, dA, \tag{23}$$

where J_H is the Hall current derived by integrating the azimuthal velocity of electrons, and the integration was conducted over the entire computational region. In this way, the impact of the finite computational region on the thrust force evaluation can be minimized because the $\boldsymbol{J} \times \boldsymbol{B}$ force produced outside of the thruster diminishes drastically as the decrease of magnetic field and plasma density. Indeed, the thrust force evaluated by ion ejection speed tends to be $5\% \sim 10\%$ lower than that of the one evaluated by Hall current. Nevertheless, the decrease of voltage utilization for ions due to the cathode sheath was not directly modeled in this study, which can influence the calculated thrust performance in terms of the inlet boundary conditions. Therefore, extending the computational region until the cathode outlet can be a possible future work for the thrust performance evaluation with even higher accuracy.

III. VALIDATION OF SIMULATION MODEL

A. Acceleration factor

In order to investigate the impact of the magnitude of the artificial mass ratio on the simulation result. The UT-SPT-62 Hall thruster was modeled with four different mass ratio cases ranging from $f^2 = 100$ to $f^2 = 2500$. The simulation and experiment results of discharge properties and thrust performances are summarized in Table III. The operation conditions of the thruster were discharge voltage 300 V, mass flow rate 1.36 mg/s, and maximum magnetic flux density 21 mT (magnetic coil current 1.5 A), and the simulation results were time-averaged over 0.1 ms. The mass ratio fraction f_B/f for each simulation cases were decided automatically according to the mass factor and the thruster operation condition as was discussed in Sec. II B. It is notable that $f_B/f = 1.0$ was used for $f^2 = 100$ case that for this condition, the mass ratio model is the same as the one used in previous study.[18]

Generally saying, all of the mass ratio cases agreed well with the measurement result. Although the simulation case with less mass factor showed better agreement with the experimental result, the discrepancies between the measured and simulated thrust and discharge current were typically less than 10%. Naturally, however, the discharge oscillation amplitude was reproduced poorly by $f^2 = 900$ and $f^2 = 2500$ cases because of the unpreserved instability frequencies as was discussed in Sec. II B, which is the compromise point of the presented mass ratio model. The axial distribution of plasma properties of potential, electron number density, and electron temperature at the channel center is presented by Fig. 7. The result of different mass factor cases agreed well with each other that the mutual discrepancy was at most 10%–15%. Moreover, the converging trend toward the $f^2 = 100$ case result was found that the discrepancy between the $f^2 = 400$ and $f^2 = 100$ cases was negligibly small. Naturally, however, employing smaller mass factor yields more accurate simulation results, the computation becomes more expensive. Therefore, the $f^2 = 2500$ case was considered to be a good compromise point of accuracy and the computational cost and was adopted in this study.

B. Mass ratio fraction

Parametric study was conducted to investigate the impact of the newly introduced mass ratio fraction f_B/f on the discharge plasma simulation results. Based on the mass factor $f^2 = 2500$ simulation case presented in Sec. III A, the mass ratio fraction was varied from 0.35 to 0.45. Note that the 0.4 was theoretically considered to be the case preserving the physics the best as shown by Fig. 2.

TABLE III. Mass factor dependence of thrust performance (discharge voltage 300 V, mass flow rate 1.36 mg/s, magnetic flux density 21 mT).

	Experiment	Simulation $f^2 = 2500$	Simulation $f^2 = 900$	Simulation $f^2 = 400$	Simulation $f^2 = 100$
Mass fraction f_B/f	…	0.4	0.47	0.55	1.0
Discharge current	1.03 A	1.03 A	1.06 A	1.03 A	1.06 A
Xe^+ beam current	…	0.74 A	0.70 A	0.64 A	0.63 A
Xe^{++} beam current	…	0.08 A	0.08 A	0.08 A	0.07 A
Thrust	15.7 mN	17.3 mN	17.4 mN	15.9 mN	15.2 mN
Discharge oscillation amplitude	0.23	0.08	0.06	0.24	0.21
Thrust efficiency	29%	35%	36%	31%	29%
Specific impulse	1180 s	1260 s	1320 s	1200 s	1210 s

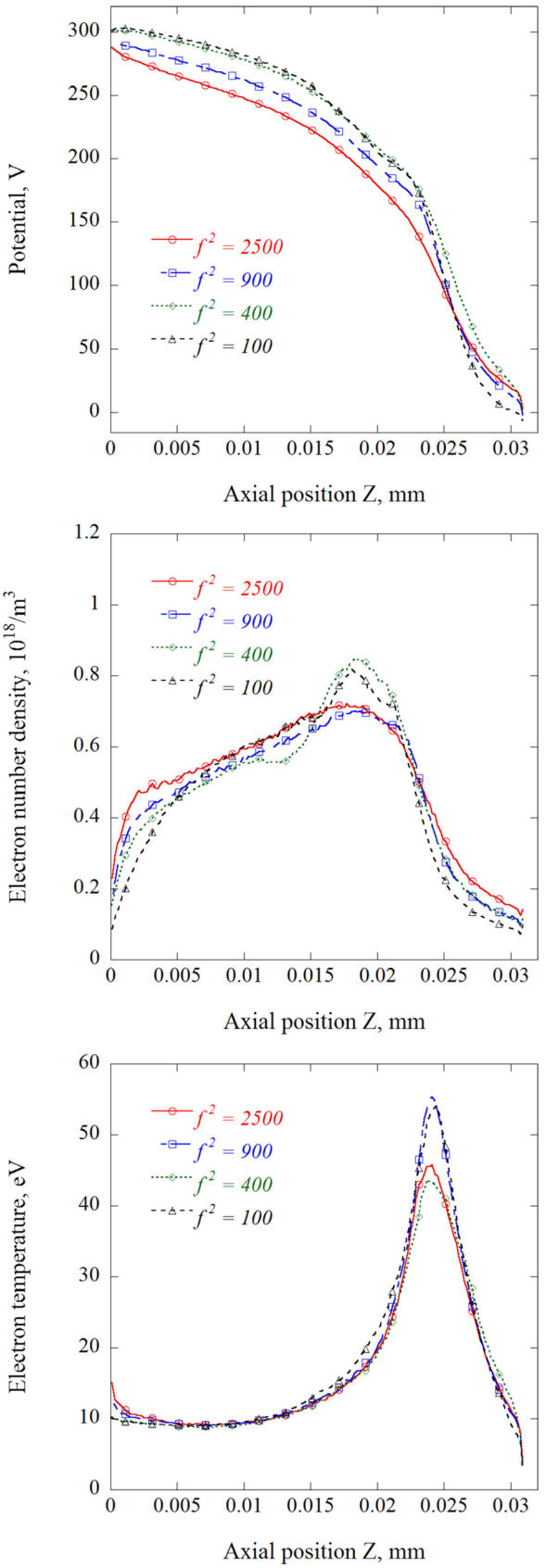

FIG. 7. Mass ratio dependence of potential (top), electron number density (middle), and electron temperature (bottom) at the channel center performance.

The simulation result of thrust performance was summarized in Table IV. The sensitivity of the mass ratio fraction was found to be insignificant that the thrust performance

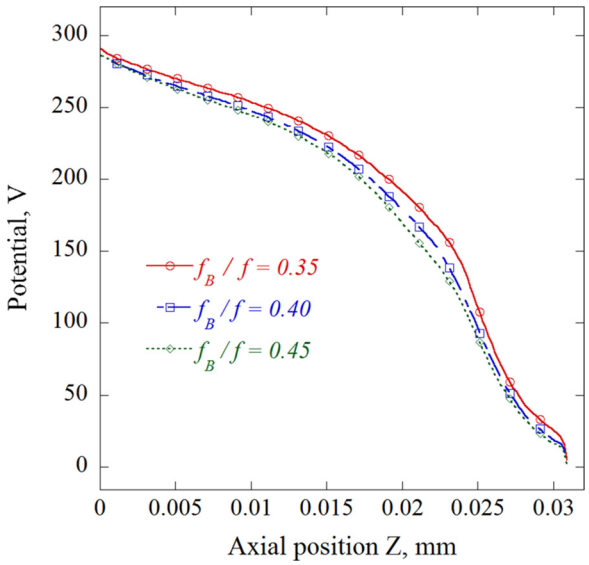

FIG. 8. Mass ratio fraction dependence of potential distribution at the channel center (Discharge voltage 300 V, mass flow rate 1.36 mg/s, magnetic flux density 21 mT).

was varied by ±5%–10% by ±12.5% change of mass ratio fraction. In addition, the potential distribution at the channel center shown by Fig. 8 also supports this conclusion. The trend was the same for other plasma property distributions that were not shown in this paper. Therefore, it can be said that the mass ratio fraction is not a predominant adjustable parameter of the computation but deduced by the consideration of electron mobility and cyclotron motion. Its impact is limited though ∼5%–10% adjustment of the simulation result is not impossible.

C. Grid spacing and macro particle size

The impact of grid spacing and the macro particle size on the discharge plasma and wall sheath structure was investigated. The simulation result was compared with the measured thrust performance and wall erosion rate.[37] Because the spatial resolution or the grid spacing is no longer restricted by the Debye length due to the semi-implicit solver, the cell size should be determined by whether the wall sheath can be resolved or not. Thus, simulation was conducted with two different grid spacing cases that one has the grid spacing equivalent to the local Debye length, whereas the other has the grid spacing 10 times larger than the Debye length. At

TABLE IV. Mass ratio fraction dependence of thrust performance.

	Experiment	Simulation $f_B/f = 0.35$	Simulation $f_B/f = 0.4$	Simulation $f_B/f = 0.45$
Mass factor f^2	…	2500	2500	2500
Discharge current	1.03 A	1.09 A	1.03 A	0.90 A
Xe^+ beam current	…	0.75 A	0.74 A	0.70 A
Xe^{++} beam current	…	0.09 A	0.08 A	0.07 A
Thrust	15.7 mN	18.3 mN	17.3 mN	16.1 mN
Oscillation amplitude	0.23	0.05	0.08	0.08
Thrust efficiency	29%	37%	35%	29%
Specific impulse	1180 s	1370 s	1260 s	1210 s

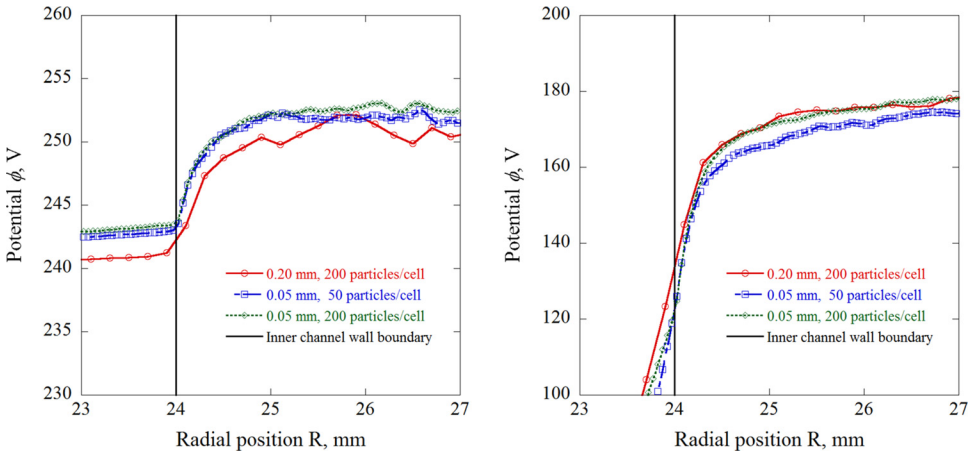

FIG. 9. Grid spacing and macro particle size dependence of wall sheath structure at 10 mm upstream from channel exit (left) and channel exit (right).

the same time, the impact of macro particle size was also investigated to evaluate the so called statistic error of the PIC simulation. Practically, three different simulation cases were test: grid spacing 0.2 mm and 200 particles per cell case, grid spacing 0.05 mm and 50 particles per cell case, and grid spacing 0.05 mm and 200 particles per cell case. The magnitude of particles/cell shown above is the approximate averaged value calculated by the total macro particle number of electrons divided by the number of cells. Practically, the variation of particles/cell was achieved by changing the macro particle size from 1.25×10^6 to 2×10^7.

The macro discharge properties were investigated, and the result is summarized in Table V. Clearly, the simulation results successfully reproduced the experimental result and the impact of grid spacing and macro particle size on the discharge properties was found to be insignificant. The simulation results of the wall sheath at the upstream channel (10 mm from channel exit) and at the channel exit are shown in Fig. 9. The time-averaged radial potential distribution at the wall vicinity, hence the dielectric wall sheath, was presented by the graphs for different conditions. Obviously, all of the simulation results agreed well with each other for both the absolute value of potential and the potential drop inside the wall sheath. The calculated sheath thickness was approximately 0.4 mm at both upstream channel and channel exit, and the potential drops were about 10 V at the upstream channel and 30 V at the channel exit. This difference of potential drop is considered to be caused by the difference of the electron temperature that the potential drop was roughly equals to the electron temperature at the sheath edge.

Fig. 10 presents the simulation result of channel wall erosion rate at the inner and outer channel for different simulation conditions. The axial position of 0.0 m denotes the anode, and channel exit is located at the position of 0.021 m. Again, the simulation result was time averaged over 0.1 ms. For both inner and outer channel, the wall erosion rates were almost identical for different grid spacing and particles per cell cases. In conclusion, all of the simulation results suggest that the grid spacing 0.2 mm is enough to achieve accurate simulation result and was adopted in this study. Additionally, the change of macro particle size only yielded trivial variation of the simulation result so that the so called statistic error due to the limited number of macro particles per cell was considered to be small.

IV. RESULTS

A. Discharge and thrust performance

First, the magnetic flux density and Xe mass flow rate dependencies of thrust performance were modeled. The simulated thruster operation conditions were discharge voltage 300 V, mass flow rate either 1.36 or 2.04 mg/s, and the magnetic flux density ranging from 11.2 to 28 mT. The simulation conditions of Table I were used, and the mass ratio fraction was fixed to $f_B/f = 0.4$. The calculated and measured thrust performance results including discharge current, thrust, discharge oscillation amplitude, and thrust efficiency were summarized in Fig. 11. The simulation successfully reproduced the measurement result of both magnetic flux density and mass flow rate dependency. The simulated thrust and discharge current and, consequently, the thrust efficiency have shown agreement with the measured results within 10% discrepancy in most conditions. Additionally, though the quantitative agreement of discharge oscillation amplitude

TABLE V. Grid spacing and macro particle size dependence of thrust performance (discharge voltage 300 V, mass flow rate 1.36 mg/s, magnetic flux density 21 mT).

	Experiment	Grid 0.2 mm 200 particles/cell	Grid 0.05 mm 50 particles/cell	Grid 0.05 mm 200 particles/cell
Discharge current	1.03 A	1.03 A	0.97 A	0.95 A
Xe^+ beam current	…	0.74 A	0.68 A	0.68 A
Xe^{++} beam current	…	0.08 A	0.07 A	0.08 A
Thrust	15.7 mN	17.3 mN	16.7 mN	16.2 mN
Oscillation amplitude	0.23	0.08	0.09	0.09
Thrust efficiency	29%	35%	36%	36%
Specific impulse	1180 s	1260 s	1290 s	1280 s

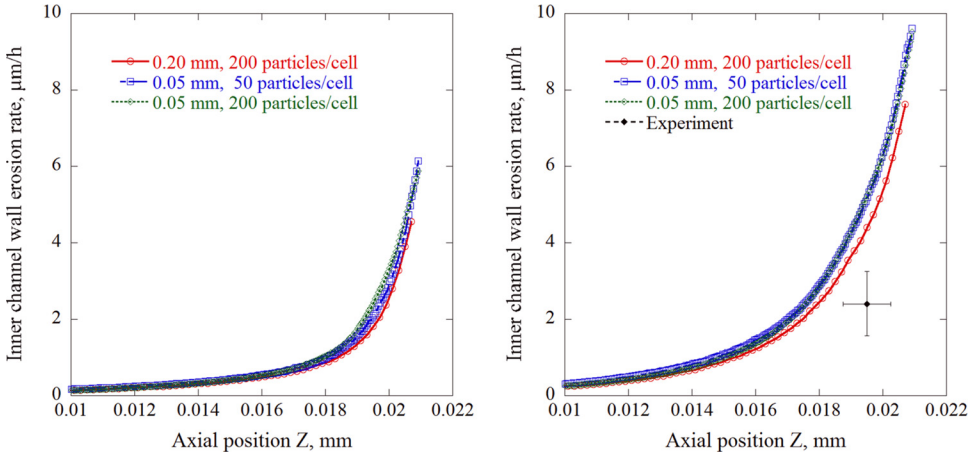

FIG. 10. Grid spacing and macro particle size dependence of wall erosion rate at the inner wall (left) and the outer wall (right).

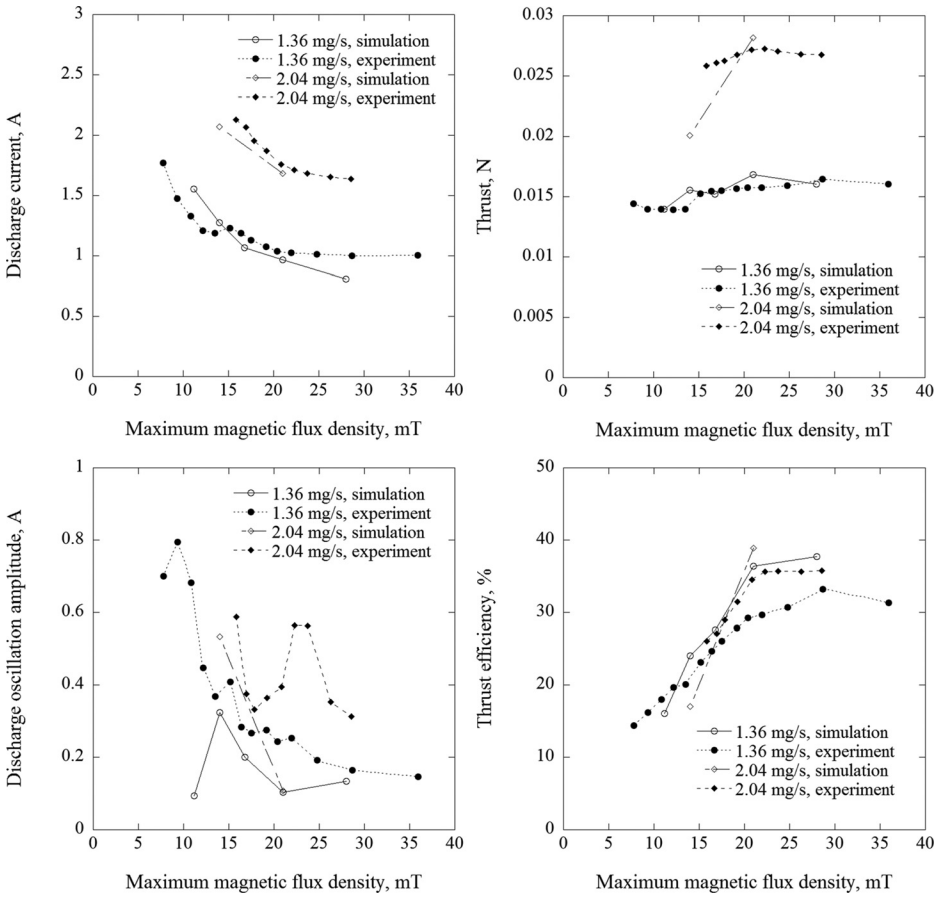

FIG. 11. Measured and simulated coil current dependence of UT-SPT-62 thrust performance, discharge current (left top), thrust (right top), discharge oscillation amplitude (left bottom), and thrust efficiency (right bottom).

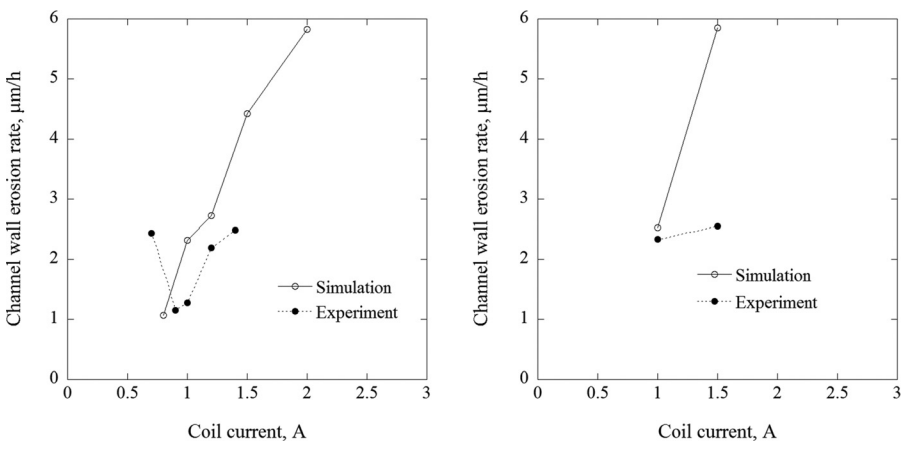

FIG. 12. Channel wall erosion rate at the outer channel wall exit of UT-SPT-62 for xenon mass flow rate 1.36 mg/s (left) and 2.04 mg/s (right).

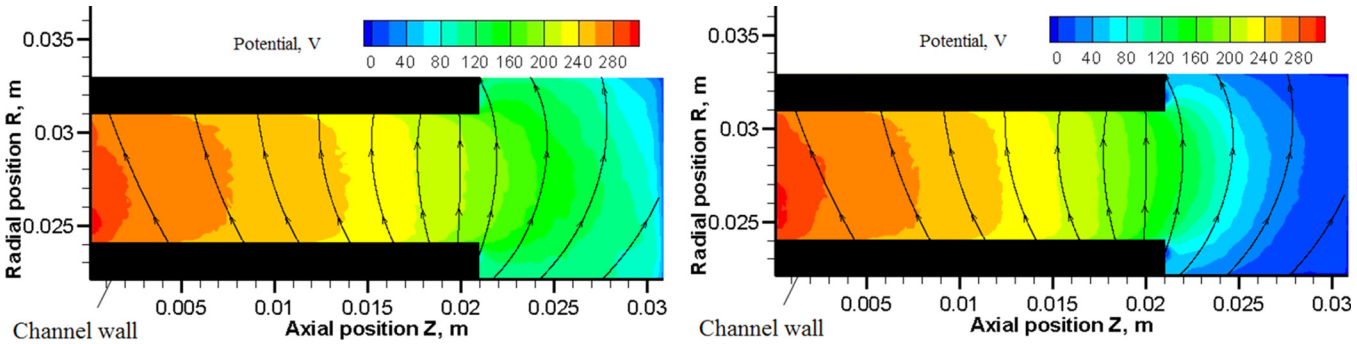

FIG. 13. Potential distribution for magnetic flux density 14 mT (left) and 21 mT (right).

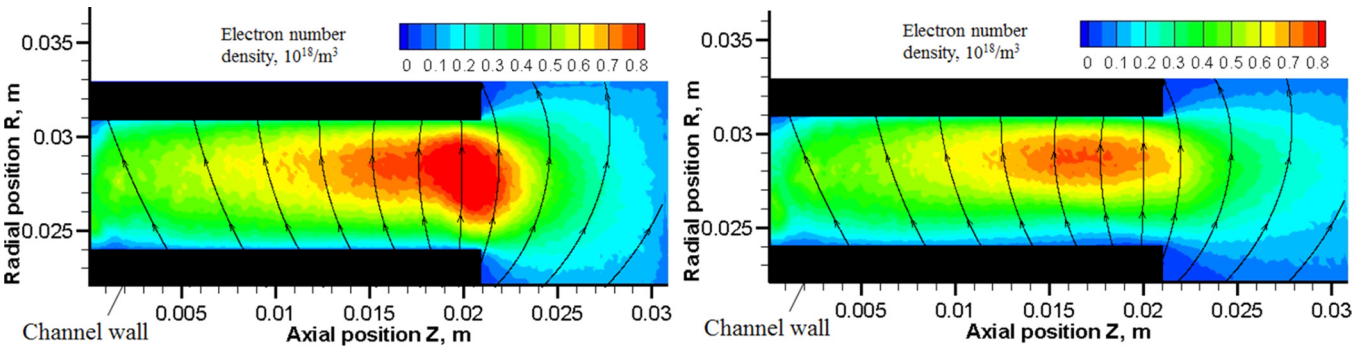

FIG. 14. Electron number density for magnetic flux density 14 mT (left) and 21 mT (right).

was rather limited, the qualitative decreasing tendency was successfully reproduced by the simulation. It is notable that this result was derived without changing any numerical parameters.

B. Begin-of-life wall erosion rate

The simulation result of the magnetic flux density mass flow rate dependencies of BOL state wall erosion rate was compared with the experimental result. Fig. 12 presents the simulated and measured[37] wall erosion rate at the channel exit (1.5 mm upstream from the corner edge) of outer channel wall. Apparently, the increasing trend of wall erosion rate as the increase of magnetic flux density was well reproduced by the simulation. This trend is unfavorable for Hall thruster operation because the thrust performance is higher in the high magnetic flux density range as was already presented in Fig. 11. The reason of this unfavorable trend can be understood by the simulation result of plasma property distributions. Figs. 13 and 14 illustrate the potential and electron number density, respectively. The stream traces denote the magnetic field lines. The calculated plasma properties suggest that as the magnetic field strength increases, the electric field inside the channel increases and the plasma will be more confined to the inner channel region. As a result, the increase of mean energy of wall loss ions caused the increase of wall erosion rate.

TABLE VI. Computational cost.

Grid spacing	Cell number	Mean macro particles/cell	Mass factor f^2	Computation time for 0.1 ms
0.05 mm	136 400	50	2500	78 h
0.05 mm	136 400	200	2500	125 h
0.20 mm	8525	200	2500	9 h
0.20 mm	8525	200	900	13 h
0.20 mm	8525	200	400	20 h
0.20 mm	8525	200	100	42 h

C. Computational cost

The computational cost of the developed model is summarized in Table VI. The computation time necessary for simulation over 0.1 ms was shown for different grid spacing, macro particle size, and mass ratio factor cases. The computational cost roughly scaled with the inverse square root of mass factor and with square of grid spacing if the number of macro particles per cell was the same. Assuming accumulative 10 times geometry updates are necessary for the lifetime simulation, and 0.2 ms is computed for each geometry, the total computation time necessary for a complete thruster life cycle can be estimated to be 180 h, which is considered to be feasible sufficiently. Or instead, for high power Hall thrusters development, the discharge and wall erosion simulation of 5 to 10 kW-class (4x diameter size) Hall can be conducted within 100 h adopting 0.2 mm grid spacing.

V. CONCLUSION

A 2D fully kinetic particle-in-cell model was presented for Hall thruster discharge and lifetime simulation. Compared with the fluid or hybrid simulation models, the presented model can directly treat the non-quasi-neutral and non-equilibrium wall sheath area. This advantage enables lifetime

modeling with increased self-consistency and accuracy because the main lifetime limiting factor of Hall thrusters is the wall erosion caused by the ion induced sputtering, which is predominated by the dielectric wall sheath and pre-sheath. Because the fully kinetic lifetime simulation was yet to be achieved so far in previous studies due to the high computational cost, the semi-implicit field solver and the technique of mass ratio manipulation was employed to accelerate the computation. However, other artificial manipulations like permittivity or geometry scaling were not used in order to avoid unrecoverable change of physics. Additionally, a new physics recovering model for the mass ratio was presented. The major advantage of the presented electron deceleration model is that the physics of electron transport across the magnetic field is preserved even for the weakly magnetically confined plasma (electron Hall parameter $\Omega_e < 100$), which is essentially important for modeling the entire thruster.

The validity of the presented model was confirmed by parametric studies over mass ration factor, the newly presented mass ratio fraction, the grid spacing, and the macro particle size. Furthermore, the thrust performance and wall erosion rate of a 600 W-class laboratory model magnetic layer type Hall thruster was modeled for different operation conditions. The simulation results successfully reproduced the measurement results typically with less than 10% discrepancy for different magnetic flux density and propellant mass flow rate cases. It is notable that this agreement was achieved without tuning any numerical parameters. Additionally, the computational cost was successfully reduced to the level that the Hall thruster fully kinetic lifetime simulation is feasible. Works are underway to model the entire lifecycle of Hall thrusters of different power levels. In summary, the presented model performed promising results for lifetime modeling and can even contribute to three dimensional kinetic modeling as the example of its possible future application.

ACKOWLEDGEMENTS

The authors express their gratitude for the support of JSPS KAKENHI Grant No. 235104.

[1]A. I. Morozov and V. V. Savelev, *Fundamentals of Stationary Plasma Thruster Theory*, Previews of Plasma Physics (Springer, US, 2000).
[2]V. A. Petrosov, A. I. Vasin, V. I. Baranov, J. R. Wetch, E. J. Britt, S. P. Wong, and R. Lin, in Proceedings of 24th International Electric Propulsion Conference, Moscow, IEPC-95-41, 1995.
[3]C. E. Garner, J. R. Brophy, J. E. Polk, and L. C. Pless, in Proceedings of the 31th AIAA Joint Propulsion Conference, San Diego, AIAA-1995-2667, 1995.
[4]K. D. Grys, A. Mathers, B. Welander, and V. Khayms, in Proceedings of the 46th AIAA Joint Propulsion Conference, Nashville, AIAA-2010-6698, 2010.
[5]W. Huang and A. D. Gallimore, in Proceedings of the 48th AIAA Joint Propulsion Conference, Atlanta, AIAA-2012-4035, 2012.
[6]K. Komurasaki and Y. Arakawa, J. Propul. Power **11**, 1317 (1995).
[7]J. M. Fife, "Hybrid-PIC modeling and electrostatic probe survey of Hall thrusters," Ph.D. dissertation (MIT, 1998).
[8]L. Garrigues, I. D. Boyd, and J. P. Boeuf, J. Propul. Power **17**, 772 (2001).
[9]G. J. M. Hagelaar, J. Bareilles, L. Garrigues, and J.-P. Boeuf, J. Appl. Phys. **91**, 5592 (2002).
[10]J. Bareilles, G. J. M. Hagelaar, L. Garrigues, C. Boniface, J. P. Boeuf, and N. Gascon, Phys. Plasmas **11**, 3035 (2004).
[11]J. T. Yim, M. Keidar, and I. D. Boyd, in Proceedings of the 42nd AIAA Joint Propulsion Conference, Sacramento, AIAA-2006-4657, 2006.
[12]S. Y. Cheng and M. Martinez-Sanchez, J. Propul. Power **24**, 987 (2008).
[13]I. G. Mikellides, I. Katz, R. R. Hofer, and D. M. Goebel, in Proceedings of the 48th AIAA Joint Propulsion Conference, Atlanta, AIAA-2012-3789, 2012.
[14]C. K. Birdsall and A. B. Langdon, *Plasma Physics via Computer Simulation* (Adam-Hilger, 1991).
[15]M. Hirakawa, Electron Transport Mechanism in a Hall Thruster, in Proceedings of 25th IEPC, Cleveland, IEPC-97-021, 1997.
[16]J. J. Szabo, "Fully kinetic numerical modeling of a plasma thruster," Ph.D. dissertation (MIT, 2001).
[17]F. Taccogna, S. Longo, M. Capitelli, and R. Schneider, Phys. Plasmas **12**, 053502 (2005).
[18]S. Yokota, K. Komurasaki, and Y. Arakawa, in Proceedings of the 42nd AIAA Joint Propulsion Conference, Sacramento, AIAA-2006-5170, 2006.
[19]J. M. Fox, "Advances in fully kinetic PIC simulation of a near-vacuum Hall thruster and other plasma systems," Ph.D. dissertation (MIT, 2007).
[20]J. C. Adam, A. Héron, and G. Laval, Phys. Plasmas **11**, 295 (2004).
[21]I. Kronhaus, A. Kapulkin, B. Natan, and M. Guelman, in Proceedings of the 32nd IEPC, Wiesbaden, IEPC-2011-043, 2011.
[22]K. Hara, I. D. Boyd, and V. I. Kolobov, Phys. Plasmas **19**, 113508 (2012).
[23]S. Cho, K. Komurasaki, and Y. Arakawa, in Proceedings of the 48th AIAA Joint Propulsion Conference, Atlanta, AIAA-2012-4016, 2012.
[24]S. A. Oghienko, V. D. Olendarev, and S. V. Veryutin, in Proceedings of the 48th AIAA Joint Propulsion Conference, AIAA-2012-4181, 2012.
[25]Y. Raitses, M. Griswold, L. Ellison, J. Parker, and N. J. Fisch, in Proceedings of the 48th AIAA Joint Propulsion Conference, AIAA-2012-4179, 2012.
[26]D. Escobar and E. Ahedo, in Proceedings of the 48th AIAA Joint Propulsion Conference, AIAA-2012-4180, 2012.
[27]R. J. Mason, J. Comput. Phys. **41**, 233–244 (1981).
[28]V. Viel-Inguimbert, in Proceedings of the 28th IEPC, Toulouse, IEPC-2003-258, 2003.
[29]K. P. Subramanian and V. Kumar, J. Phys. B **20**, 5505 (1987).
[30]M. Hayashi, J. Phys. D: Appl. Phys. **16**, 581 (1983).
[31]F. J. de Heer, R. H. J. Jansen, and W. van der Kaay, J. Phys. B **12**, 979 (1979).
[32]R. W. Wagenaar and F. J. de Heer, J. Phys. B **13**, 3855 (1980).
[33]C. Achenbacht, A. Mullert, E. Salzbornt, and R. Becker, J. Phys. B **17**, 1405 (1984).
[34]Y. Garnier, V. Viel, J. F. Roussel, and J. Bemard, J. Vac. Sci. Technol. A **17**, 3246 (1999).
[35]Y. Yamamura and H. Tawara, At. Data Nucl. Data Tables **62**, 149 (1996).
[36]B. Rubin, J. L. Topper, and A. P. Yalin, J. Appl. Phys. **42**, 205205 (2009).
[37]S. Cho, S. Yokota, K. Komurasaki, and Y. Arakawa, J. Propul. Power **29**, 278 (2013).